AUT Journal of Electrical Engineering

AUT J. Elec. Eng., 53(1) (2021) 99-110
DOI:10.22060/eej.2021.19196.5383

Analysis of Nano-Wires at Terahertz and Optical Frequencies Using Surface Impedance Models

A. Gholipour[1]

[1]Assistant Professor, School of Electrical Engineering, University of Shahid Beheshti, Tehran, Iran

ABSTRACT: Different surface impedance models are applied to circular nano-wires at terahertz and optical frequencies and the accuracy of these surface impedance boundary conditions (SIBCs) is studied. The simplest form of SIBC defines a local relation between the tangential electric and magnetic equivalent surface currents at each point on the boundary. This definition is very dependent on the constituent material of the wire and its radius. The generalized IBC (GIBC) improves the accuracy of the local definition by considering the curvature of the surface at each observation point. On the other hand, the operator definition of the surface impedance presented in the SIGO method (surface impedance generating operator), is an exact field theoretical approach that determines the relation between equivalent electric and magnetic surface currents. Moreover, this method is suitable for parallel processing. For the special case of circular wires, the SIGO operator is derived. To validate the SIBC models, the results are compared with the SIGO. In spite of its extreme simplicity, it is observed that the accuracy of SIBC models is limited at optical and terahertz frequencies. It is also shown that some forms of SIBCs presented in the literature for nano-wires can be considered as special cases of SIGO formulation.

Review History:
Received: Oct. 31, 2020
Revised: Jan. 16, 2021
Accepted: Jan. 16, 2021
Available Online: Jun. 01, 2021

Keywords:
Surface impedance boundary condition
Surface integral equation
Method of moment
Nano-wire, Plasmonics

1- INTRODUCTION

Metals are good conductors of microwave and millimeter wave frequencies. At lower frequencies, these materials can be modeled as perfect electric conductors (PECs). On the other hand, at terahertz and optical frequencies, the good conductor approximation would no longer be valid. Metals at these frequencies are penetrated by the fields, and act like lossy dielectrics whose index of refractions are imaginary with a negative real part. The boundary condition on PECs enforces the tangential components of the total electric field to be zero. The total electric field is actually defined as the sum of the incident and scattered electric fields. On a good conductor, the tangential components of the total electric field can be related to the equivalent surface electric current:

$$\bar{E}_{tot} = Z_S \bar{J}_s \tag{1}$$

where Z_S is the surface impedance. This equation is obviously a local definition.

For an infinitely thick conductor the Z_S is obtained as [1]:

$$Z_S = (1+j)\frac{1}{\sigma\delta} \tag{2}$$

where σ is the conductivity of the medium and δ is the skin depth:

$$\delta = \sqrt{\frac{2}{\omega\mu\sigma}} \tag{3}$$

Generally, regardless of the direction of incidence, the impinging plane wave is transmitted into the conductor perpendicular to its surface. Moreover, the surface impedance of a good conductor has equal real and imaginary parts.

Although Eq. (3) is derived for infinitely thick conductor, this Z_S is widely used for analyzing microstrip circuits. However, for high accuracy applications, other models of microstrip conductor loss are proposed [2]. It is worth mentioning that we cannot use the boundary condition (1), if we have no accurate guess about the value of the surface impedance Z_S.

Applying the boundary condition (1) to the microstrip circuits greatly reduces the size of the problem and the simulation time by relaxing the field analysis inside the conductors. If we can apply the impedance boundary condition at the interface of other material types, then we can benefit from the same kind of simplification too.

The surface impedance boundary condition (SIBC) toward this goal is defined as [3]:

$$\hat{n} \times \bar{E}_{tot} = Z_S \hat{n} \times \hat{n} \times \bar{H}_{tot} \tag{4}$$

*Corresponding author's email: a_gholipour@sbu.ac.ir

This equation is a local relation between the tangential components of the electric and magnetic fields. This boundary condition can considerably reduce the simulation time and computational burden, but this definition of surface impedance seriously depends on the Z_S value at the observation point. Unfortunately, the exact value of Z_S will remain unknown, unless the total electric and magnetic fields are determined. Conversely, knowing the fields, we do not need Z_S anymore. In practice, the use of the SIBC (4) is limited to those problems for which we know the Z_S with acceptable accuracy. A common choice of Z_S is the characteristic impedance of the illuminated medium or scatterer:

$$Z_S \approx Z_c = \sqrt{\frac{j\omega\mu}{\sigma + j\omega\varepsilon}} \tag{5}$$

It is worth mentioning that the good conductors have very high σ. Hence, for this type of materials, Eq. (5) is reduced to (2). By defining the equivalent surface electric current J_S as:

$$\bar{J}_s = \hat{n} \times \bar{H}_{tot} \tag{6}$$

we can also obtain Eq. (1) form Eq. (4).

The validity of Eq. (5), depends on the constitutive parameters of the scatterer and its geometry. To improve the accuracy, different methods have been proposed in the literature. In [4,5], the Z_C is computed separately for TM and TE polarizations following a two steps procedure. In the first step, the field distributions on the boundary of rectangular wires are calculated. Then, the surface impedance for TM and TE polarizations are derived by dividing the respective components of the already found tangential fields. It is actually a useful tool for analyzing complex THz and optical structures, because after finding the surface impedance of the wire as a function of location, one is able to replace this wire with its computed surface impedance and hence, considerably simplify the problem.

To improve the accuracy, in [3,6] generalized IBC (GIBC) for a scalar function U is defined:

$$\sum_{m=0}^{M}\sum_{l=0}^{m}\sum_{k=0}^{m-l} c_{klm} \frac{\partial^m}{\partial x^{m-l-k}\partial y^k \partial z^l} U = 0 \tag{7}$$

where $U(x,y,z)$ can be the normal component of an electromagnetic field or an acoustic velocity potential.

As a matter of fact, due to the presence of derivatives, the preceding boundary condition relates the tangential electric field at each point not only to the tangential magnetic field at the same point, but also to the tangential magnetic fields at the vicinity of that point. This definition somehow includes more information of the impedance relation, hence, lead to better approximation compared with Eq. (4). In [7,8] the global form of IBC was introduced. For the specific case of 2D rectangular wires, the fields on the wire cross section are discretized using the finite difference time domain (FDTD) in order to find the relation among the tangential components of the fields on the boundary. The resulting matrix representation of surface impedance is more accurate than both SIBC and GIBC, although its use is limited to the problems with separable TE/TM solutions.

The surface impedance generating operator (SIGO) is the most accurate way of defining impedance boundary condition. This operator is defined as [9]:

$$Z(\mathbf{r},\mathbf{r}') = -j\omega\mu\, \hat{n} \times \bar{\mathbf{G}}_e(\mathbf{r},\mathbf{r}') \tag{8}$$

where $\bar{\mathbf{G}}_e$ denotes electric dyadic Green's function of second type. This dyadic representation of surface impedance is theoretically exact for any finite scatterer with an arbitrary shape. However, its practical use would be limited to those problems for which the required dyadic Green's function can be obtained analytically.

The SIBC model can be used to analyze the bodies of revolution, though it may encounter some limitations due to the curvature of these types of scatterers. In [10] the surface impedance is derived and used to study the nano-wire dipoles at optical frequencies. In [11, 12] the circular wires take the role of terahertz waveguides, which are analyzed using the surface impedance model.

In the current paper, we study the circular wires at terahertz and optical frequencies using the surface impedance formulations. First, the operator form of the surface impedance is derived for these structures. Following the results, the validity of other representations of surface impedance for circular wires are studied. It is shown that the definitions that are presented in the literature [10, 13, 14] can be handled as a special case of the SIGO formulation.

The rest of the paper is organized as follows. In section 2, the SIGO formulation is derived for the 2D circular wires. In section 3 the exterior integral equation is introduced and is combined with the derived operator surface impedance. Later, the final single source integral equation is implemented using the method of moments (MoM). Section 4 illustrates the numerical results. Concluding remarks are presented in section 5.

2- SIGO FORMULATION FOR 2D CIRCULAR WIRE

The cross section of a circular wire with no variation with respect to longitudinal direction, which is supposed to be aligned along with the z direction, is shown in Figure 1 together with the applied SIGO boundary conditions. For the excitations that do not change in the longitudinal direction, we are encountered with a 2D scattering problem. Fig. 1-a shows the SIGO boundary condition for TM polarized incident wave while Fig. 1-b demonstrates the boundary condition of TE case.

In the following subsections, both cases are considered and studied using the SIGO formulation.

2-1- the TM Case

The field components of TM_z modes are $H\varphi$, $H\rho$ and Ez, given that $\partial/\partial z = 0$. These field components are the

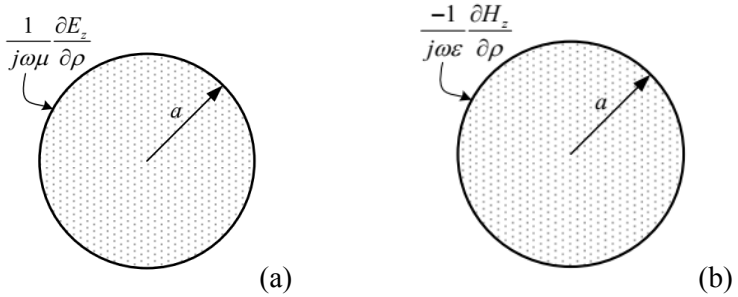

Fig. 1. The cross section of the wire and the respective boundary conditions defined in SIGO method, a) TM case, b) TE case.

functions of ρ and φ and satisfy the Helmholtz equation. To be meticulous in our derivations, we define the position vector of source (observation) points as:

$$\overline{r}_G' = \overline{R}_{OO'} + \overline{r}_g' \tag{9}$$

where $\overline{r}_g'$ is the position vector described in local coordinate system and $\overline{R}_{OO'}$ determines the position vector of the origin of the local coordinate system defined in the global coordinate system. Generally, in our notations the subscript *g* denotes the local coordinate while subscript *G* emphasizes that the used coordination system is global.

For a circular wire, when the center of the circular cross section is located at the origin of the local coordinate system, the position vector of each point on the boundary is expressed as:

$$\overline{r}_g = \rho_g \hat{\rho}_g = x_g \hat{x}_g + y_g \hat{y}_g = a\cos\varphi_g \hat{x}_g + a\sin\varphi_g \hat{y}_g \tag{10}$$

where a is the radius of the wire under study and φ' denotes the angle in polar system.

For the electric field we can write:

$$\frac{1}{\rho_g}\frac{\partial}{\partial\rho_g}\left(\rho_g \frac{\partial E_z}{\partial\rho_g}\right) + \frac{1}{{\rho_g}^2}\frac{\partial^2 E_z}{\partial{\varphi_g}^2} + k^2 E_z = 0 \tag{11}$$

where k is the complex wave number inside the wire:

$$k = \sqrt{-j\omega\mu(j\omega\varepsilon + \sigma)} \tag{12}$$

The boundary condition enforced by SIGO method is stated as:

$$\frac{1}{j\omega\mu}\frac{\partial E_z}{\partial\rho_g} = J_{sz} \tag{13}$$

The required dyadic Green's function in this case has only one component, which is the solution of the following boundary value problem:

$$\begin{cases} \dfrac{1}{\rho_g}\dfrac{\partial}{\partial\rho_g}\left(\rho_g \dfrac{\partial G^{zz}}{\partial\rho_g}\right) + \dfrac{1}{{\rho_g}^2}\dfrac{\partial^2 G^{zz}}{\partial{\varphi_g}^2} + k^2 G^{zz} = \\ \dfrac{1}{\rho_g}\delta(\rho_g - \rho_g')\delta(\varphi_g - \varphi_g') \\ \left.\dfrac{\partial G^{zz}(\rho_g,\varphi_g;\rho_g',\varphi_g')}{\partial\rho_g}\right|_{\rho_g = a} = 0 \end{cases} \tag{14}$$

Different techniques have been introduced with the aim of finding dyadic Green's functions. These techniques lead to different representations for the same dyadic Green's functions. Series expansion is one of the methods. By applying this method to the equation (14), we can express G^{zz} as:

$$G^{zz}(\rho_g,\varphi_g;\rho_g',\varphi_g') = \sum_{p=-\infty}^{+\infty} g_p(\rho_g;\rho_g',\varphi_g')e^{jp\varphi_g} \tag{15}$$

For finding $g_p(\rho_g;\rho_g',\varphi_g')$, the preceding equation is substituted in (14):

$$\sum_{p=-\infty}^{+\infty}\left[\frac{\partial^2}{\partial{\rho_g}^2} + \frac{1}{\rho_g}\frac{\partial}{\partial\rho_g} - \frac{p^2}{{\rho_g}^2} + k^2\right] g_p(\rho_g;\rho_g',\varphi_g')e^{jp\varphi} = \frac{1}{\rho_g}\delta(\rho_g - \rho_g')\delta(\varphi_g - \varphi_g') \tag{16}$$

Using the orthogonality of the set of $\{e^{-jq\varphi}\}$ functions for integer values of q, we can reduce the equation (16) in the form of:

$$\left[\frac{\partial^2}{\partial{\rho_g}^2} + \frac{1}{\rho_g}\frac{\partial}{\partial\rho_g} + (k^2 - \frac{p^2}{\rho^2})\right] g_p(\rho_g;\rho_g',\varphi_g') = \frac{1}{\rho_g}\delta(\rho_g - \rho_g')\frac{e^{jp\varphi_g'}}{2\pi} \tag{17}$$

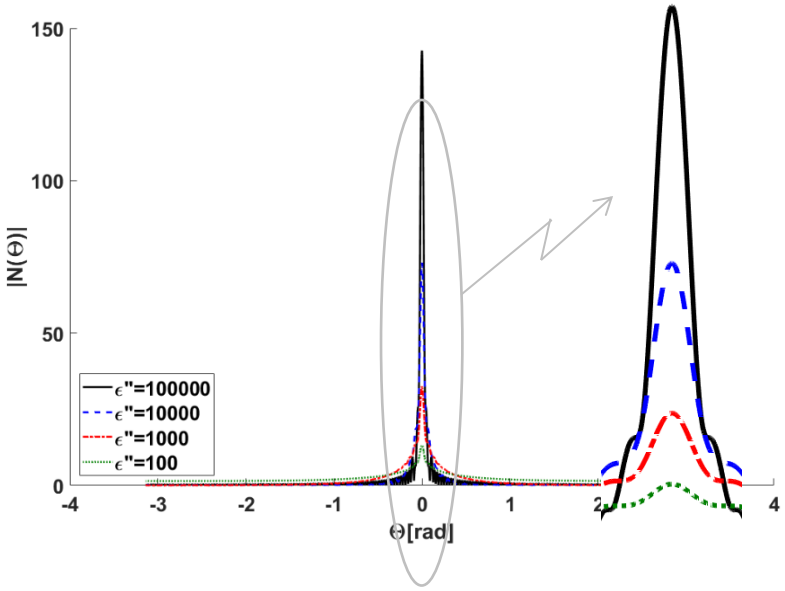

Fig. 2. The magnitude of function N(Θ) as defined in (25) for materials with different conductivities.

The general solutions of this ordinary differential equation are:

$$g_p^{(1)} = A_p J_p(k\rho_g) \qquad \rho_g < \rho_g' \qquad (18)$$

$$g_p^{(2)} = B_p \left[J_p(k\rho_g) - \frac{J_p'(ka)}{Y_p'(ka)} Y_p(k\rho_g) \right] \qquad \rho_g > \rho_g' \qquad (19)$$

The Wronskian of these solutions is:

$$W(\rho_g') = \mathrm{A}_p \, B_p \, \frac{-J_p'(ka)}{Y_p'(ka)} \frac{2}{\pi\rho_g'} \qquad (20)$$

Finally, g_p is found as:

$$g_p(\rho_g;\rho_g',\varphi_g') = \begin{cases} \dfrac{-1}{4}\left[J_p(k\rho')Y_p'(ka) - J_p'(ka)Y_p(k\rho_g')\right] & \\ \dfrac{J_p(k\rho_g)}{J_p'(ka)} e^{-jp\varphi_g'} & \rho_g < \rho_g' \\ \dfrac{-1}{4}\left[J_p(k\rho_g)Y_p'(ka) - J_p'(ka)Y_p(k\rho_g)\right] & \\ \dfrac{J_p(k\rho_g')}{J_p'(ka)} e^{-jp\varphi_g'} & \rho_g > \rho_g' \end{cases} \qquad (21)$$

Consequently, the solution of G^{zz} is obtained as:

$$G^{zz}(\rho_g;\rho_g',\varphi_g') = \begin{cases} \dfrac{\left[J_p(k\rho')Y_p'(ka) - J_p'(ka)Y_p(k\rho_g')\right]}{\dfrac{-1}{4}\displaystyle\sum_{p=-\infty}^{+\infty} \frac{J_p(k\rho_g)}{J_p'(ka)} e^{jp(\varphi_g-\varphi_g')}} & \rho_g < \rho_g' \\ \dfrac{\left[J_p(k\rho_g)Y_p'(ka) - J_p'(ka)Y_p(k\rho_g)\right]}{\dfrac{-1}{4}\displaystyle\sum_{p=-\infty}^{+\infty} \frac{J_p(k\rho_g')}{J_p'(ka)} e^{jp(\varphi_g-\varphi_g')}} & \rho_g > \rho_g' \end{cases} \qquad (22)$$

For both source and observation points located on the boundary, we can simplify the preceding expression and write it as:

$$G^{zz}(\varphi_g - \varphi_g') = \frac{-1}{2\pi ka} \sum_{p=-\infty}^{+\infty} \frac{J_p(ka)}{J_p'(ka)} e^{jp(\varphi_g-\varphi_g')} \qquad (23)$$

The electric field on the boundary of circular wire can be related to the equivalent surface electric current using SIGO equation:

$$E_z\big|_C = \frac{j\omega\mu}{2\pi ka} \oint_{C'} \left(\sum_{p=-\infty}^{+\infty} \frac{J_p(ka)}{J_p'(ka)} e^{jp(\varphi_g-\varphi_g')} \right) J_{sz}(\varphi_g')dl' \qquad (24)$$

Defining the function *N(Θ)* as:

$$N(\Theta) = \sum_{p=-\infty}^{+\infty} \frac{J_p(ka)}{J_p'(ka)} e^{jp\Theta} \qquad (25)$$

We can write:

$$E_z\big|_C = \frac{j\omega\mu}{2\pi k} \int_0^{2\pi} J_{sz}(\varphi_g')N(\varphi_g - \varphi_g')d\varphi_g' \qquad (26)$$

Fig. 2 shows the $|N(\Theta)|$ for different materials with high conductivities. It is observed that at $\Theta=0$ the function takes the maximum and behaves like an impulse function for highly conducting materials. By approximating *N(Θ)* with Delta function in the limit, we can simplify the preceding equation as:

$$E_z \simeq \frac{j\omega\mu}{2\pi k} \frac{J_0(ka)}{J_0'(ka)} H_\varphi = -j \frac{\omega\mu}{2\pi k} \frac{J_0(ka)}{J_1(ka)} H_\varphi \qquad (27)$$

Therefore, the surface impedance can be defined as:

$$Z_s \simeq -j\frac{\omega\mu}{k}\frac{J_0(ka)}{J_1(ka)} \tag{28}$$

The above equation clearly shows that the local surface impedance is obtained as a limiting case of the SIGO approach. A similar equation has been found in [10, 13], albeit in completely different contexts.

2-2- TE Case

In this case, the electric field of the incident plane wave has generally both $\hat{\rho}$ and $\hat{\varphi}$ components. Hence, the electric dyadic Green's function generally has four components:

$$\bar{\bar{G}}_e = G_e^{\rho\rho}\hat{\rho}\hat{\rho} + G_e^{\rho\varphi}\hat{\rho}\hat{\varphi} + G_e^{\varphi\rho}\hat{\varphi}\hat{\rho} + G_e^{\varphi\varphi}\hat{\varphi}\hat{\varphi} \tag{29}$$

We can use the auxiliary Green's function of g_m^{zz} and follow the procedure described in [15] to find $\bar{\bar{G}}_e$.

For the problem at hand, g_m^{zz} satisfies the following boundary value problem stated in local coordinate system as:

$$\begin{cases} \nabla^2 g_m^{zz}(\mathbf{r},\mathbf{r}'') + k^2 g_m^{zz}(\mathbf{r},\mathbf{r}'') = -\dfrac{1}{\rho_g}\delta(\rho_g-\rho_g'')\delta(\varphi_g-\varphi_g'') \\ g_m^{zz}\big|_{\rho_g=a} = 0 \end{cases} \tag{30}$$

The solution of the preceding equation can be expressed as:

$$g_m^{zz}(\rho_g,\varphi_g;\rho_g'',\varphi_g'') = \frac{1}{4}\begin{cases} \sum_{p=-\infty}^{+\infty}\dfrac{\left[J_p(k\rho_g'')Y_p(ka)-J_p(ka)Y_p(k\rho_g'')\right]}{J_p(ka)}e^{jp(\varphi_g-\varphi_g'')} & \rho_g<\rho_g'' \\ \sum_{p=-\infty}^{+\infty}\dfrac{\left[J_p(k\rho_g)Y_p(ka)-J_p(ka)Y_p(k\rho_g)\right]}{J_p(ka)}e^{jp(\varphi_g-\varphi_g'')} & \rho_g>\rho_g'' \end{cases} \tag{31}$$

$$= \sum_{p=-\infty}^{+\infty} g_{p\rho}^{zz}(\rho_g;\rho_g'')e^{jp(\varphi_g-\varphi_g'')}$$

Consequently, G_m can be computed as:

$$\bar{\mathbf{G}}_m(\mathbf{r},\mathbf{r}') = \int \bar{\mathbf{g}}_m(\mathbf{r},\mathbf{r}'')\cdot\nabla''\times\bar{\mathbf{I}}\delta(\mathbf{r}'-\mathbf{r}'')dv'' \tag{32}$$

which yields the following dyadic components:

$$G_m^{z\rho}(\mathbf{r},\mathbf{r}') = \sum_{p=-\infty}^{+\infty}\frac{jp}{\rho_g'}g_{p\rho}^{zz}(\rho_g;\rho_g')e^{jp(\varphi_g-\varphi_g')} \tag{33}$$

$$G_m^{z\varphi}(\mathbf{r},\mathbf{r}') = -\sum_{p=-\infty}^{+\infty}\frac{\partial\left[g_{p\rho}^{zz}(\rho_g;\rho_g'')\right]}{\partial\rho_g''}\bigg|_{\rho_g''=\rho_g'}e^{jp(\varphi_g-\varphi_g')} \tag{34}$$

Finally, we can find G_e from:

$$\bar{\mathbf{G}}_e(\mathbf{r},\mathbf{r}') = \frac{1}{k^2}\left[\bar{\mathbf{G}}_{e0}(\mathbf{r},\mathbf{r}') - \bar{\mathbf{I}}\delta(\mathbf{r}-\mathbf{r}')\right] \tag{35}$$

where I is the unitary dyad and:

$$\bar{\mathbf{G}}_{e0}(\mathbf{r},\mathbf{r}') = \nabla\times\bar{\mathbf{G}}_m(\mathbf{r},\mathbf{r}') \tag{36}$$

By substituting (33) and (34) in (36), the components of G_{e0} are calculated:

$$G_{e0}^{\rho\rho} = \sum_{p=-\infty}^{+\infty}\frac{-p^2}{\rho_g\rho_g'}g_{p\rho}^{zz}(\rho_g;\rho_g')e^{jp(\varphi_g-\varphi_g')} \tag{37}$$

$$G_{e0}^{\varphi\rho} = \sum_{p=-\infty}^{+\infty}\frac{jp}{\rho_g'}\frac{\partial g_{p\rho}^{zz}(\rho_g;\rho_g')}{\partial\rho_g}e^{jp(\varphi_g-\varphi_g')} \tag{38}$$

$$G_{e0}^{\rho\varphi} = \sum_{p=-\infty}^{+\infty}\frac{jp}{\rho_g}\frac{\partial\left[g_{p\rho}^{zz}(\rho_g;\rho_g'')\right]}{\partial\rho_g''}\bigg|_{\rho_g''=\rho_g'}e^{jp(\varphi_g-\varphi_g')} \tag{39}$$

$$G_{e0}^{\varphi\varphi} = \sum_{p=-\infty}^{+\infty}\frac{\partial}{\partial\rho_g}\frac{\partial\left[g_{p\rho}^{zz}(\rho_g;\rho_g'')\right]}{\partial\rho_g''}\bigg|_{\rho_g''=\rho_g'}e^{jp(\varphi_g-\varphi_g')} \tag{40}$$

Having G_e computed, one can relate the electric field on the boundary of wire to the equivalent surface electric current using SIGO equation [9]:

$$\mathbf{E}(\mathbf{r}) = j\omega\mu\int\bar{\mathbf{G}}_e(\mathbf{r},\mathbf{r}')\cdot\mathbf{J}_s(\mathbf{r}')dr' \;;\; \mathbf{r}\in V_n, \mathbf{r}'\in S_n \tag{41}$$

Using (8), we can represent (41) for the tangential field components as:

$$-\hat{n}\times\mathbf{E}(\mathbf{r}) = \mathrm{Z}(\mathbf{r},\mathbf{r}')\bullet\mathbf{J}_s(\mathbf{r}')\;;\; \mathbf{r},\mathbf{r}'\in S_n \tag{42}$$

Therefore, unlike the definition of surface impedance in [10, 13] that are limited to TM polarization, SIGO is able to represent the surface impedance for TE polarization as well.

Please note that in local coordinate system, the surface equivalent electric current on circular wire has only $\hat{\varphi}_g$ component, and only two components of $\bar{\bar{G}}_e = G_e^{\rho\varphi}\hat{\rho}_g\hat{\varphi}_g + G_e^{\varphi\varphi}\hat{\varphi}_g\hat{\varphi}_g$ would be effective in finding electric field from (41). It is worth mentioning that equation (41), which determines the relation between the electric field and the surface equivalent electric current can be transformed to a global coordinate system after being first derived in the local coordinate system of each scatterer.

For the 2D problem of infinitely long wire with no variation with respect to the longitudinal direction, one is able to study the TE polarized waves easier using the duality. However, we aim to show that the SIGO formulation is general and is capable of handling general scattering problems, by the

derivations above.

3- EXTERIOR PROBLEMS:

The integral equations (26) or (41) cannot be solved for finding the unknown equivalent electric surface currents unless the exterior problem is considered. The electric field integral equation of exterior problem for a penetrable obstacle enclosed by surface S is stated as [16]:

$$-\mathbf{E}_{inc}(\mathbf{r}) = \bar{L}_{1E}(\mathbf{r},\mathbf{r}')\bullet\mathbf{J}_S(\mathbf{r}') + \bar{K}_{1E}(\mathbf{r},\mathbf{r}')\bullet\mathbf{M}_S(\mathbf{r}')\ ;\ \mathbf{r},\mathbf{r}'\in S \quad (43)$$

Where $\boldsymbol{J}_S$ and $\boldsymbol{M}_S$ denote the equivalent electric and magnetic surface currents and:

$$\bar{L}_{1E}(\mathbf{r},\mathbf{r}') = -j\omega\mu_1(\bar{I} + \frac{\nabla\nabla}{k_1^2})\, g_1(\mathbf{r},\mathbf{r}') \quad (44)$$

$$\bar{K}_{1E}(\mathbf{r},\mathbf{r}') = -\nabla g_1(\mathbf{r},\mathbf{r}')\times\bar{I} \quad (45)$$

where $\bar{I}$ is the unitary dyadic Green's function and g_1 for a 2D problem is expressed as:

$$g_1(\mathbf{r},\mathbf{r}') = \frac{1}{4j}H_0^2(k_1|\bar{\rho}-\bar{\rho}'|) \quad (46)$$

Considering that $\mathbf{M}_S = -\hat{n}\times\mathbf{E}$, one can combine (42) and (43) and introduce a kind of single source integral equation. For a problem with multiple scatterers, the resulting equation is expressed as:

$$-\bar{E}_{inc}(\mathbf{r}) = \sum_{S_1}^{S_N} L_{1E}(\mathbf{r},\mathbf{r}')\bullet\bar{J}_S(\mathbf{r}') + \sum_{S_1}^{S_N} K_{1E}(\mathbf{r},\mathbf{r}')\bullet Z_n(\mathbf{r}',\mathbf{r}'')\bullet\bar{J}_S(\mathbf{r}'')\ ;$$
$$\mathbf{r}\in S_{tot};\mathbf{r}',\mathbf{r}''\in S_n \quad (47)$$

where N is the number of scatterers with surfaces S_1 to S_N and S_{tot} is defined as $S_{tot} = \bigcup_{n=1}^{N} S_n$. For each scatterer, the operator form of surface impedance, $Z_n(\mathbf{r}',\mathbf{r}'')$, is calculated separately. This single source integral equation can be solved to find the surface equivalent electric current. Having the equivalent current J_S known, using (47), we can find the field everywhere outside the scatterers.

We use the method of moment to change the integral equations into matrix equations and find the unknown coefficients.

For the special case of TM polarization, the equivalent current on each circular wire can be described as:

$$\bar{J}_S(\bar{\rho}') = J_{sz}(\varphi_g') \quad (48)$$

By expanding the equivalent surface electric currents with 1D pulse basis functions of P_n we have:

$$J_{sz}^i(\varphi_g') = \sum_{n=1}^{N}\alpha_n^i P_n(\varphi_g') \quad (49)$$

where superscript i denotes the ith scatterer and α_n^i s are its unknown coefficients. The vector of all unknowns put together can be written as:

$$[\alpha_n] = \begin{bmatrix}[\alpha_n^1]\\ [\alpha_n^2]\\ \vdots\end{bmatrix} \quad (50)$$

By combining the interior and exterior problems, we solve the final single source equation to find these coefficients.

4- NUMERICAL RESULTS:

As a first example, the fields scattered by a single circular wire immersed in free space is studied. Two different material types (i.e. dielectric and metal) are considered and the equivalent electric current in each case is computed for both models of: a) the SIBC defined by (27) and b) the SIGO model (26). The radius of the wire is supposed to be $a=0.6\lambda_0$, where λ_0 is the wavelength of the incident plane wave in free space. In the following simulations, λ_0=800nm is considered. Fig. 3 shows the computed surface equivalent electric currents for the dielectric wire. It is clear that the SIBC model completely fails to predict the correct distribution of equivalent electric current. However, the operator surface impedance model can accurately trace the analytical solution. The convergence of the SIGO solution is also observed in the Figure. It's been granted that with only 18 segments the result obtained using the SIGO method agrees with the analytical solution very well.

Fig. 4 compares the results obtained using the mentioned methods when the wire is made of gold. Material property is taken from [17], where the complex permittivity of *-24.06-1.5j* is found for gold at λ_0=800nm. In this case, the SIBC model gives better predictions of the equivalent electric current. We expected this result, as the SIBC model becomes more accurate when the conductivity of scatterer increases. Regardless, the SIGO model shows better performance. It converges rapidly, so with *N=180* the difference between SIGO and analytical results is hardly visible.

For comparing the results obtained by different methods quantitatively, the following criteria is defined:

$$\xi = \frac{\oint_c \left|J_{sz}^{Anal}(\varphi') - J_{sz}^{Numer}(\varphi')\right|^2 d\varphi'}{\oint_c \left|J_{sz}^{Anal}(\varphi')\right|^2 d\varphi'} \quad (51)$$

where J_{sz}^{Anal} is the analytical solution and J_{sz}^{Numer} is the equivalent current computed numerically by applying

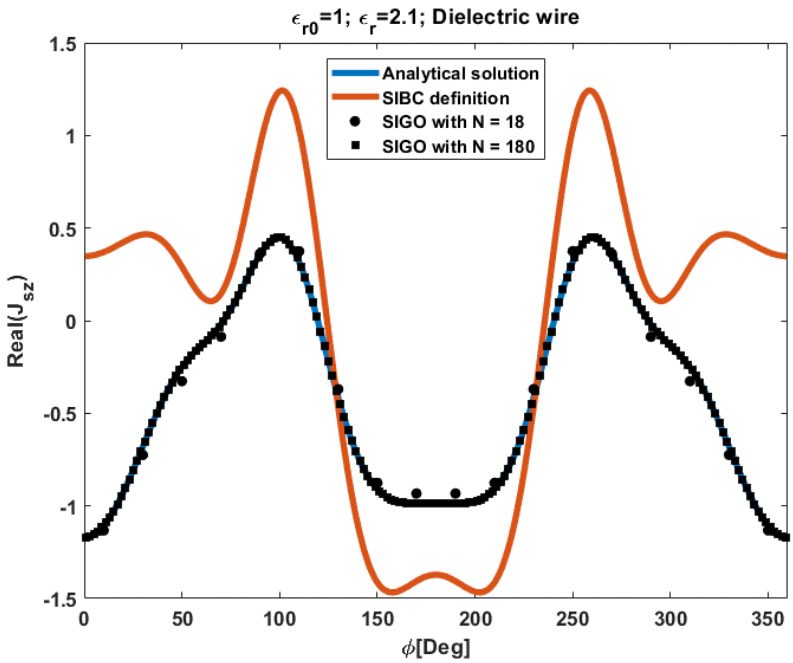

(a)

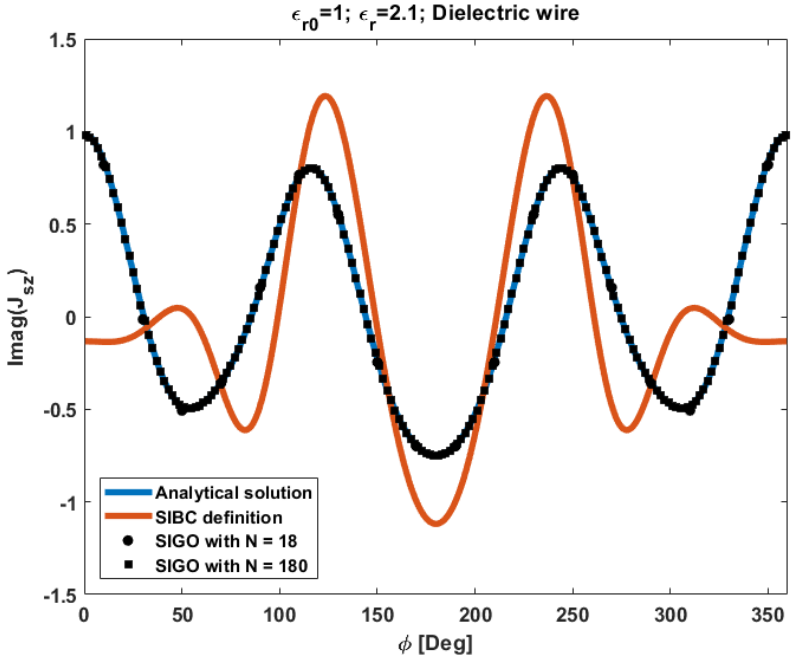

(b)

Fig. 3. The distribution of equivalent electric current on a typical dielectric circular wire with radius $a=0.6\lambda_0$, a) the real part, b) the imaginary part

the SIBC or SIGO boundary conditions. Table 1 shows the calculated ξ, which quantifies the error for different methods. As it is expected, the SIGO method is more accurate for having less ξ.

After finding the equivalent electric and magnetic surface currents accurately, it is a common task to calculate the scattered fields following the equivalence principle. Fig.5 and 6 show that the equivalent magnetic currents for both

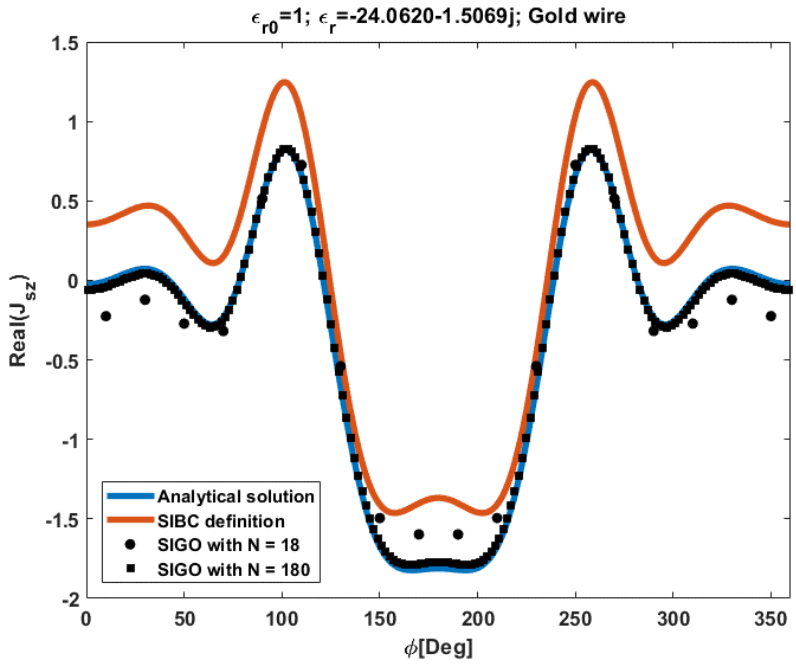

(a)

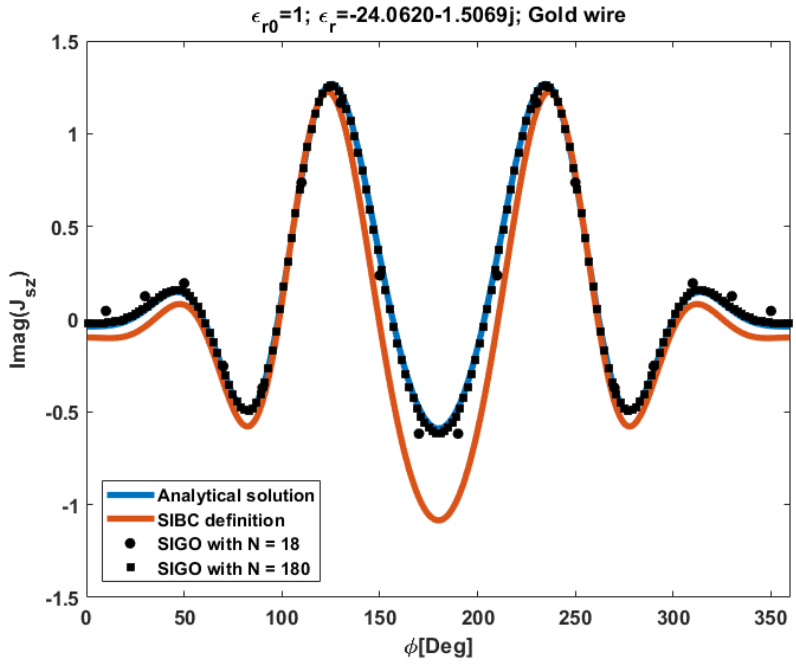

(b)

Fig. 4. The distribution of equivalent electric current on a typical metal circular wire with radius $a=0.6\lambda_0$ at optical frequencies, a) the real part, b) the imaginary part

dielectric and gold wires are found accurately by the SIGO formulation. The scattered fields are also plotted in Fig.7 and 8.

The next example analyzes the current distribution on the wires when three wires are configured as shown in Fig. 9. The rods are placed close to each other. Fig. 10 illustrates the current distribution on the right hand side wire. The real part of the equivalent current is plotted in Fig. 10-a, and the imaginary part is shown in Fig. 10-b. Outstanding convergence is observed in the solution of SIGO model.

Table 1. calculated ξ for different methods

	Complex permittivity	SIBC	SIGO- 18 points	SIGO- 180 points
Dielectric	2.1	1.082	4.0e-3	2.95e-05
Gold	-24.06-j1.5	1.61e-1	2.7e-2	7.43e-04

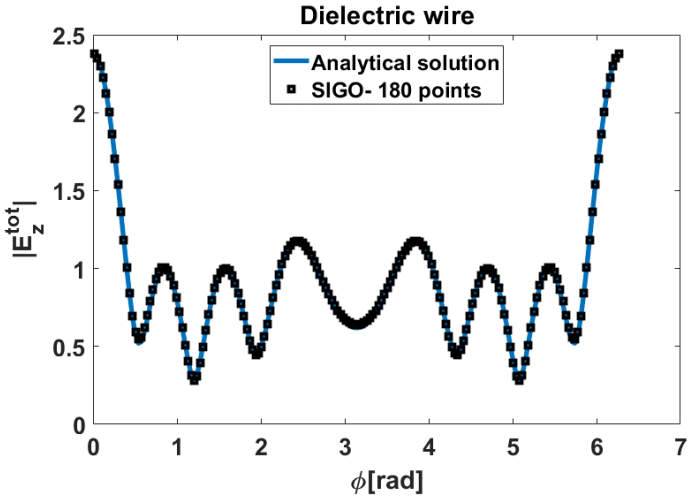

Fig. 5. Total electric field right on the boundary for dielectric circular nano-wire

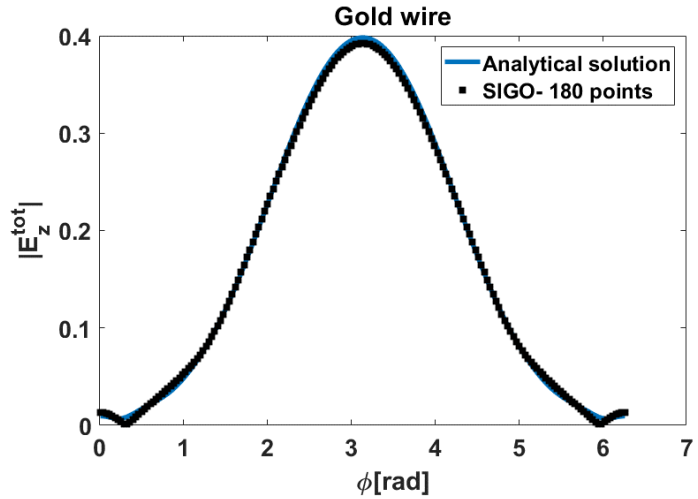

Fig. 6. Total electric field right on the boundary for gold nano-wire

5- CONCLUSIONS

Different surface impedance models were applied to the problem of scattering from circular wires at optical frequencies. It was elicited that the local definition has limited accuracy and cannot be used for studying the problems in which the scatterer is penetrated by the fields. On the other hand, the operator definition is theoretically exact and is able to handle both dielectric and metal optic problems accurately. The SIGO formulation that actually defines the operator expression of the surface impedance was used to find the distribution of equivalent currents. Two examples were considered. In the first example, a single wire was analyzed, for which the analytical solution exists. It was shown that the SIGO method is accurate even for coarse meshing. The convergence of SIGO solution was also investigated in a three wires configuration. Very good convergence was achieved. Probing the operator expression of surface impedance gives an evidence for the expected accuracy of the local definitions.

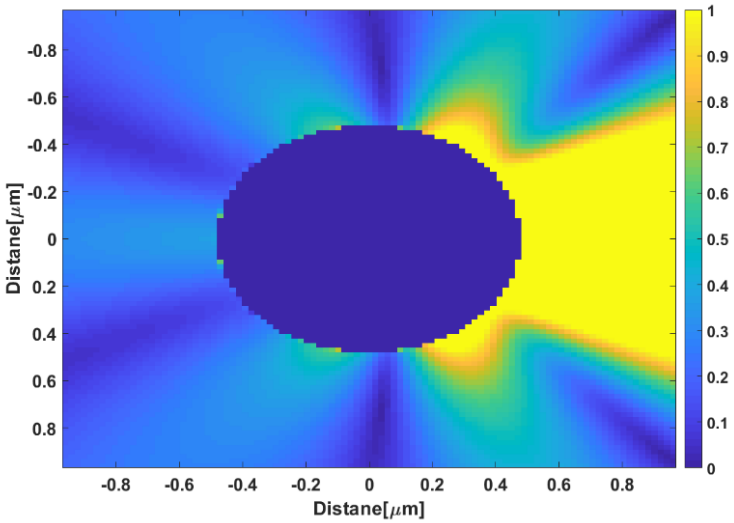

Fig. 7. Scattered field by dielectric nano-wire

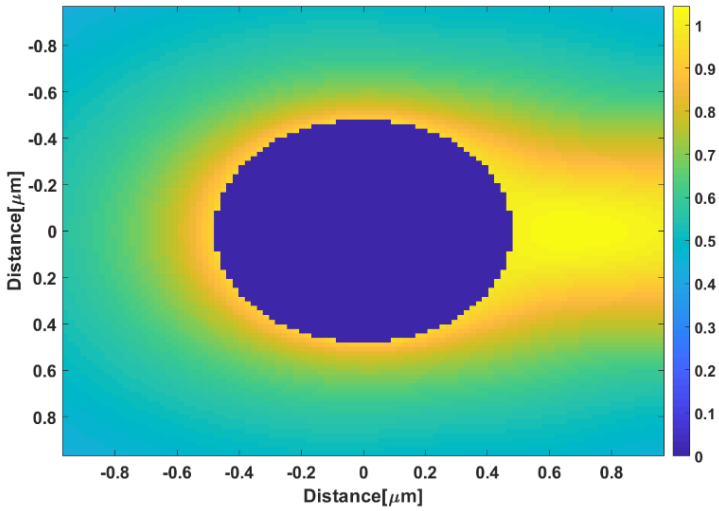

Fig. 8. Scattered field by gold nano-wire

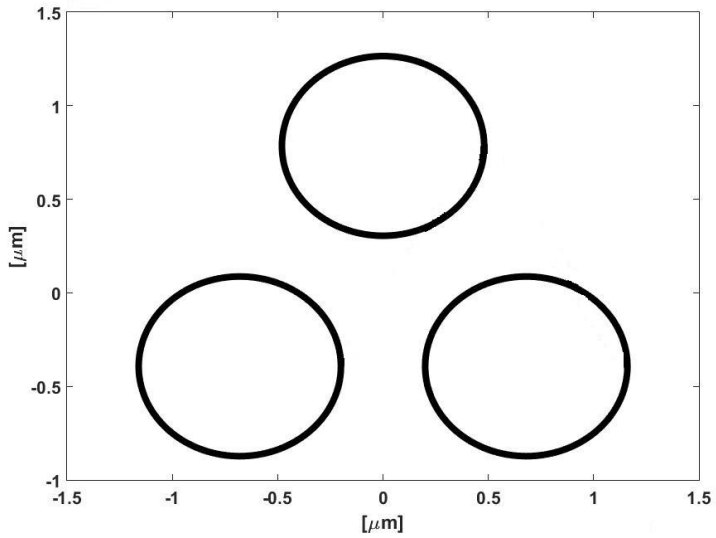

Fig. 9. The geometry of three gold wires with radius $a=0.6\lambda_0$ studied as the second example

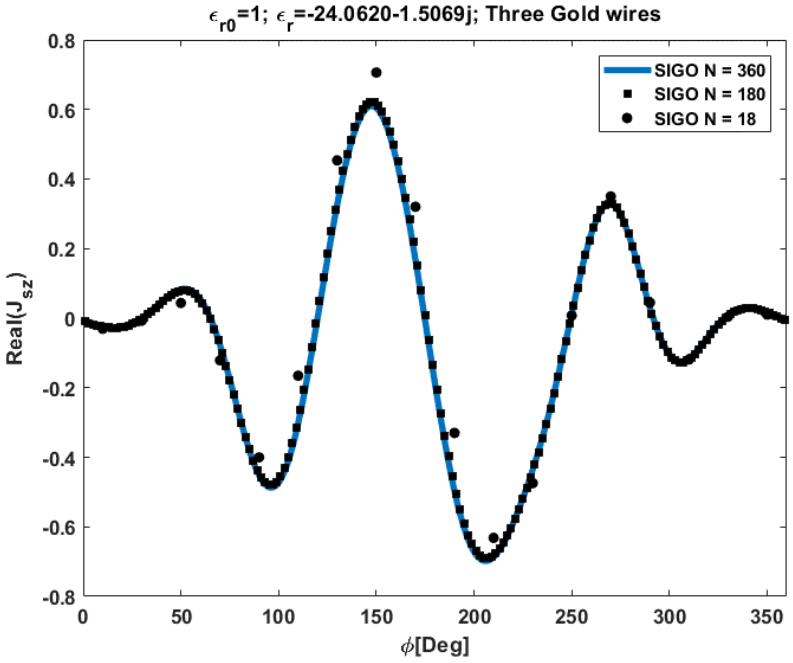

(a)

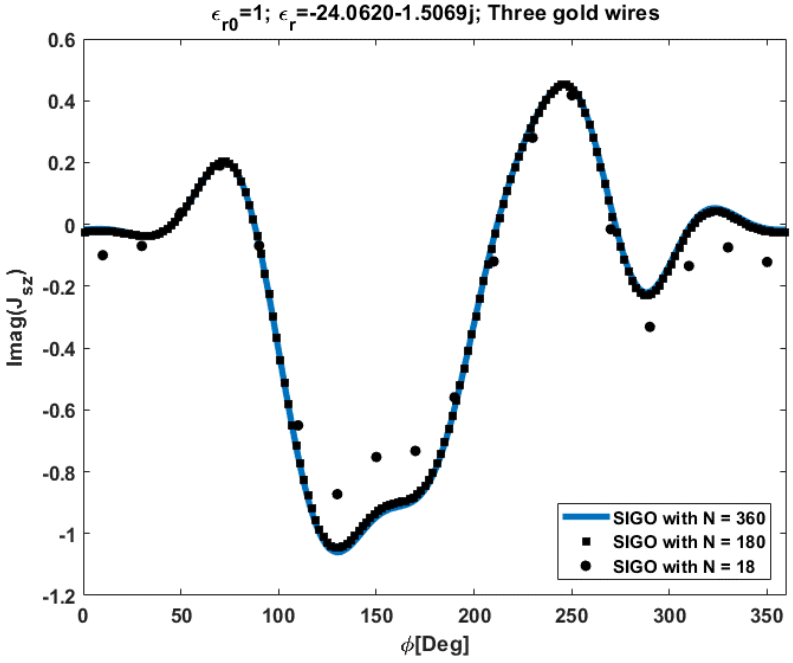

(b)

Fig. 10. The distribution of equivalent electric current on the right hand side wire of Fig. 5, a) the real part, b) the imaginary part

REFERENCES:

[1] Simon Ramo, John R. Whinnery and Theodore Van Duzer, Fields and Waves in Communication Electronics, Wiley, 1994.

[2] Rautio, James C., and Veysel Demir. "Microstrip conductor loss models for electromagnetic analysis." IEEE transactions on microwave theory and techniques 51, no. 3 (2003): 915-921.

[3] T. B. A. Senior, J. L. Volakis, Aproximate boundary conditions in electromagnetic, The Institution of Electrical Engineering, 1995.

[4] Gholipour, Alireza, Reza Faraji-Dana, Guy AE Vandenbosch, and Safieddin Safavi-Naeini. "Surface impedance modeling of plasmonic circuits at optical communication wavelengths." Journal of lightwave technology 31, no. 20 (2013): 3315-3322.

[5] Gholipour, Alireza, and Shokrollah Karimian. "Rectangular Nano-Wire Analysis at Terahertz and Optical Frequencies Using Interior-Exterior Method and Surface Impedance Model." In 2019 2nd West Asian Colloquium on Optical Wireless Communications (WACOWC), pp. 143-146. IEEE, 2019.

[6] T. B. a. Senior and J. L. Volakis, "Generalized impedance boundary conditions in scattering," Proc. IEEE, vol. 79, no. 10, pp. 1413–1420, 1991.

[7] K. Coperich and A. C. Cangellaris, "Enhanced skin effect for partial-element equivalent-circuit (PEEC) models," Microw. Theory Tech. IEEE Trans., vol. 48, no. 9, pp. 1435–1442, 2000.

[8] Shiquan He; Sha, W.E.I.; Lijun Jiang; Choy, W.C.H.; Weng Cho Chew; Zaiping Nie; "Finite-Element-Based Generalized Impedance Boundary Condition for Modeling Plasmonic Nanostructures," Nanotechnology, IEEE Trans., vol. 11, no. 2, pp. 336–345, 2012.

[9] Gholipour, Alireza, Reza Faraji-Dana, and Guy AE Vandenbosch. "High performance analysis of layered nanolithography masks by a surface impedance generating operator." JOSA A 34, no. 4 (2017): 464-471.

[10] G. Hanson, "On the applicability of the surface impedance integral equation for optical and near infrared copper dipole antennas," Antennas Propagation, IEEE Trans., vol. 54, no. 12, pp. 3677–3685, 2006.

[11] K. Wang and D. Mittleman, "Dispersion of surface plasmon polaritons on metal wires in the terahertz frequency range," Phys. Rev. Lett., vol. 157401, no. April, pp. 1–4, 2006.

[12] J. Yang, Q. Cao, C. Zhou1, "Analytical Recurrence Formula for the Zeroth-order Metal Wire Plasmon of Terahertz Waves," J. Opt. Soc. Am. A, Vol. 27, No.7, July 2010.

[13] L. Knockaert, P. Van den Abeele, and D. De Zutter, "Surface impedance of cylinders and wedges: A Neumann approach," Int. J. Electron. Commun., vol. 53, no. 1, pp. 11–17, 1999.

[14] L. Knockaert and D. De Zutter, "Integral equation for the fields inside a dielectric cylinder immersed in an incident E-wave," Antennas Propagation, IEEE Trans., vol. 34, no. 8, pp. 1065–1067, 1986.

[15] Gholipour, A. "Analysis of optical nanostructures using the surface impedance generating operator." JOSA B 37, no. 2 (2020): 295-303.

[16] Weng Cho Chew, Mei Song Tong and Bin Hu, Integral Equation Methods for Electromagnetic and Elastic Waves, Morgan, 2009.

[17] A. D. Rakić, A. B. Djurišic, J. M. Elazar, and M. L. Majewski. Optical properties of metallic films for vertical-cavity optoelectronic devices, Appl. Opt. 37, 5271-5283 (1998)

HOW TO CITE THIS ARTICLE

Gholipour, A. Analysis of Nano-Wires at Terahertz and Optical Frequencies Using Surface Impedance Models. AUT J. Elec. Eng., 53(1) (2021) 99-110.

DOI: 10.22060/eej.2021.19196.5383